Structure of Cholesterol/Ceramide Monolayer Mixtures: Implications to the Molecular Organization of Lipid Rafts

Luana Scheffer,* Inna Solomonov,† Markus Jan Weygand,‡ Kristian Kjaer,‡ Leslie Leiserowitz,† and Lia Addadi*
*Department of Structural Biology, Weizmann Institute of Science, Rehovot, Israel; †Department of Materials and Interfaces, Weizmann Institute of Science, Rehovot, Israel; and ‡Materials Research Department, Risø National Laboratory, Roskilde, Denmark

ABSTRACT The structure of monolayers of cholesterol/ceramide mixtures was investigated using grazing incidence x-ray diffraction, immunofluorescence, and atomic force microscopy techniques. Grazing incidence x-ray diffraction measurements showed the existence of a crystalline mixed phase of the two components within a range of compositions of cholesterol/ceramide between 100:0 and 67:33. The mixed phase coexists with the ceramide crystalline phase in the range of compositions between 50:50 and 30:70; between 30:70 and 0:100 only the highly crystalline phase of ceramide was detected. The latter was determined and modeled. Immunolabeling was performed with an antibody specific to the cholesterol monohydrate crystalline arrangement. The antibody recognizes crystalline cholesterol monolayers, but does not interact with crystalline ceramide. Immunofluorescence and atomic force microscopy data show that in uncompressed ceramide monolayers, the highly crystalline phase coexists with a disordered loosely packed phase. In contrast, no disordered phase coexists with the new crystalline mixed phase. We conclude that the new mixed phase represents a stable homogeneous arrangement of cholesterol with ceramide. As ceramide incorporates the lipid backbone common to all sphingolipids, this arrangement may be relevant to the understanding of the molecular organization of lipid rafts.

INTRODUCTION

Cholesterol-sphingolipid interactions are fundamental for lipid bilayer formation in cellular membranes, yet they are still not well understood. A significant advance in the understanding of membrane organization, function, and structure developed with the suggestion that plasma membranes of animal cells may contain laterally segregated domains, the so-called ''lipid rafts'' (Simons and Ikonen, 1997). This new concept emerged as a modification of the conventional ''fluid mosaic model'', presenting the lipid bilayer as a homogeneous mixture of cholesterol and lipids, with proteins interspersed and freely diffusing (Singer and Nicolson, 1972). Lipid rafts, in contrast, are thought to be formed by dynamical clustering of cholesterol and sphingolipids, particularly sphingomyelin, in organized structures. These domains appear to be immersed in a medium akin to the fluid mosaic model, where phospholipids are the main component. Receptor-mediated signaling events originate from lipid rafts (Simons and Toomre, 2000; Smart et al., 1999), whereas many proteins colocalize with them in the membrane, and are thus thought to be preferentially partitioned in the rafts (Brown and Rose, 1992).

Evidence for the existence of cholesterol-rich domains in cell membranes has accumulated within the last few years. A wide range of techniques was applied, providing information about the presence and distribution of cholesterol-rich domains in cell membranes, their size, and their dynamics at different spatial resolutions. (Friedrichson and Kurzchalia, 1998; Giocondi et al., 2000; Pralle et al., 2000; Varma and Mayor, 1998).

The majority of sphingolipids consist of a sphingosine backbone linked through amide bonds to long-chain fatty acids to yield ceramide (Fig. 1). Different classes of sphingolipids result upon attachment of different headgroups to the terminal hydroxyl of ceramide. The most abundant sphingolipid in the animal cell membranes is sphingomyelin, which, due to the phosphorylcholine moiety attached to the ceramide backbone, is considered the sphingolipid analog of phosphatidylcholine. The bulky phosphorylcholine moiety of sphingomyelin protrudes from the membrane into the water, whereas the ceramide backbone interacts with the other lipids forming the membrane bilayer.

The raft-associated acid sphingomyelinase cleaves off the phosphorylcholine moiety of sphingomyelin, thus leading to in situ release of ceramide (Schneider and Kennedy, 1967). Ceramide is thus considered by itself a component of lipid rafts, both strongly associating to and stabilizing the liquid-ordered state (Xu et al., 2001).

Cholesterol, the most abundant sterol in animal tissues, is an essential constituent of cell membranes and lipoprotein particles. It is composed of a steroid ring system, with little conformational flexibility, terminated with a 3β-hydroxyl group (Fig. 1). Cholesterol partitions between lipid rafts and the disordered lipid homogeneous phase, but shows higher affinity for saturated sphingolipids than for unsaturated phospholipids (Ramstedt and Slotte, 2002). It is considered a key component of lipid rafts and its concentration is a determining factor in raft stability.

Submitted August 25, 2004, and accepted for publication January 26, 2005.

Address reprint requests to Prof. Lia Addadi, Dept. of Structural Biology, Weizmann Institute of Science, Rehovot 76100, Israel. E-mail: lia.addadi@weizmann.ac.il.

0006-3495/05/05/3381/11 $2.00

doi: 10.1529/biophysj.104.051870

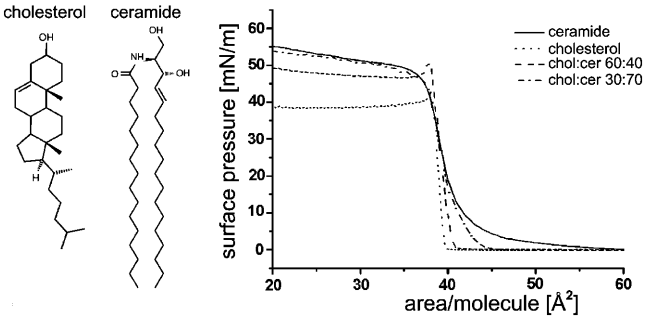

FIGURE 1 Surface pressure-molecular area isotherms of pure cholesterol, pure ceramide, and two mixtures thereof. The GIXD measurements were carried out at low surface pressures, corresponding to a surface area/molecule of 40-45 Å^2 for pure ceramide and of 38.5-40 Å^2 for the others.

The proposed structural model for lipid rafts involves a liquid-ordered assembly of sphingolipids, where cholesterol is thought to be intercalated between the long, saturated acyl chains of the lipids (Simons and Ikonen, 1997). Both cholesterol and ceramide are thought to stabilize the raft by ''diluting'' the repulsive interactions that would ensue between the bulky sphingolipid headgroups in the water phase (Huang and Feigenson, 1999; Majewski et al., 2001).

The proposed model, however, assumes a unique lipid composition and structure for the rafts, which is not necessarily correct. It thus appears necessary to determine the composition and the molecular arrangement of the various components within the domains on a more individual scale. What is the molecular organization of the rafts? Are they uniform entities with the same molecular organization? Is the component distribution within one domain homogeneous? These are only few out of the many questions still not answered that are important for the understanding of the functioning of cholesterol-rich domains in general.

The tight interaction inferred between cholesterol and the long saturated alkyl chains of the sphingolipids, explains the resistance of the cholesterol-rich domains to detergent extraction at 4°C, which is the most widely used biochemical tool for identifying lipid rafts (Brown and London, 1997). With the detergent approach, however, it is not possible to determine the size or structure of the domains or to distinguish between different compositions, since the membrane domains rearrange into larger detergent-resistant membranes during the treatment (Giocondi et al., 2000).

A new approach is most likely required for characterizing the molecular parameters of the component arrangement within the domains.

In this study, mixed cholesterol-ceramide monolayers were chosen as a model system to glean some information on packing arrangements of lipids. Their two-dimensional structure was solved by grazing incidence x-ray diffraction (GIXD). In addition, antibodies that were raised and selected against crystals of cholesterol monohydrate were used.

GIXD has proven to be a reliable method for determining the structure and size of ordered arrays of monolayers and multilayers of crystalline amphiphilic molecules at the air/water interface (Als-Nielsen et al., 1989; Kuzmenko et al., 2001; Jensen and Kjaer, 2001). Recently, monolayers and multilayers of cholesterol have been investigated (Rapaport et al., 2001). The sensitivity of the method, however, progressively decreases with reduced ordering.

The use of specific antibodies as reporters of the structure of organized arrays of molecules was initiated in the laboratory of one of us (L.A.) with a series of studies on specific monoclonal antibodies, isolated after exposure of organisms to crystals such as cholesterol-monohydrate and others (Geva et al., 2003; Kessler et al., 1996; Perl-Treves et al., 1996). These antibodies interact with the crystal and with organized monolayers of cholesterol at the air/water interface (Izhaky and Addadi, 2000). They do not interact with the isolated molecule or with monolayers of other steroids, such as cholestenone or epicholesterol (Geva et al., 2001). Molecular modeling of various antibody binding sites displayed chemical and geometrical complementarity between the antibodies and the specific molecular organizations they bind to (Kessler et al., 1999). Hence, it is at least conceivable that antibodies can be used as reporters of the specific molecular organization they were selected for, or the absence thereof (Addadi et al., 2003; Kruth et al., 2001).

In all likelihood, lipid rafts have local order. Various methods, GIXD, atomic force microscopy (AFM), and immunofluorescence, complement each other here, providing a structural description of single layers composed of mixtures of cholesterol and ceramide, as an initial attempt to get insight into structures of lipids that may result, in the future, to be relevant for the understanding of the organization of lipid rafts.

MATERIALS AND METHODS

N-palmitoyl-D-*erythro*-sphingosine (C16 ceramide) was purchased from Avanti Polar Lipids (Birmingham, AL). Cholesterol (>99%), rhodamine_B isothiocyanate, octadecyltrichlorosilane (OTS), as well as solvents, were purchased from Sigma-Aldrich (Rehovot, Israel). ImmunoPure IgM purification kit 44897 was purchased from Pierce (Rockford, IL). The Centricon centrifugal filter devices were acquired from Millipore (Bedford, MA). Dialysis was carried out using Spectra/Por membranes from Spectrum Medical Industries (Los Angeles, CA) with a molecular weight cutoff in the range 12,000-14,000 Da against PBS (phosphate-buffered saline). Highly oriented pyrolitic graphite (HOPG) grade SPI-2 was purchased from SPI Supplies (West Chester, PA).

The uncompressed monolayers were viewed under epifluorescent light with rhodamine filter (575 nm), in a Zeiss optical microscope, equipped with a video camera attached to an LIS-700 integration amplifier (Applitec, Holon, Israel) that allows amplification of the image intensity up to 3000×.

Lipid/chloroform solutions (~0.1 mg/ml) were used to form the monolayer films at the air/water interface for surface pressure molecular area (π-A) isotherms and GIXD measurements.

The isotherms were recorded at 5°C for each of the monolayers using a Mini LB Trough (KSV Instruments, Helsinki, Finland) with a Wilhelmy plate.

GIXD

The GIXD experiments were performed on the liquid surface diffractometer at the undulator BW1 beam line at the HASYLAB synchrotron source, DESY (Hamburg, Germany). The monolayers were formed at room temperature on a film of water ~0.25 mm thick covering a smooth glass surface, to reduce the amplitude of surface capillary waves. X-ray diffraction measurements were performed thereon upon cooling to 5°C. For all the monolayers studied by GIXD, the surface pressure was zero. A monochromatic x-ray beam ($\lambda = 1.304$ Å) was adjusted to strike the liquid surface at an incident angle α_i approximately equal to $0.85\alpha_c$, where α_c is the critical angle for total external reflection; this maximizes surface sensitivity. The dimensions of the footprint of the incoming x-ray beam on the liquid surface were ~2 × 50 mm. The scattered intensity was collected by means of a position-sensitive detector (PSD), which intercepts photons over the range $0.0 < q_z < 1.1$ Å^{-1}, q_z being the out-of-plane component of the scattering vector $\boldsymbol{q}$;

$$q_z = (2\pi/\lambda)[\sin(\alpha_i) + \sin(\alpha_f)] \approx (2\pi/\lambda)\sin(\alpha_f),$$

where α_i and α_f are the angles of the incident and diffracted beams with the horizontal plane. The measurements were performed by scanning the PSD across the horizontal component q_{xy} of the scattering vector $\boldsymbol{q}$;

$$q_{xy} = (2\pi/\lambda)[\cos^2(\alpha_i) + \cos^2(\alpha_f) - 2\cos(\alpha_i)\cos(\alpha_f)\cos(2\theta_{xy})]^{1/2}$$
$$\approx (2\pi/\lambda)[1 + \cos^2(\alpha_f) - 2\cos(\alpha_f)\cos(2\theta_{xy})]^{1/2} \approx (4\pi/\lambda)\sin(2\theta_{xy}/2) + \mathrm{Order}(\alpha_f^2),$$

where $2\theta_{xy}$ is the angle between the incident and diffracted beam projected onto the horizontal plane. A more detailed explanation of the method can be found in the literature (Als-Nielsen and Kjaer, 1989; Kuzmenko et al., 2001; Jensen and Kjaer, 2001).

SHELX-97 was used for x-ray structure refinement of the GIXD data and CERIUS software was used for the construction of the molecular models.

AFM

AFM observations were carried out with the aid of a Nanoscope III Multi-Mode system (Digital Instruments, Santa Barbara, CA). Microfabricated square-pyramidal shaped tips of silicon nitride (Digital Instruments) were used. In situ tapping-mode imaging under MilliQ water was performed by using a standard fluid cell and the wide-legged cantilever (nominal spring constant, 0.58 N/m). The best results were obtained at a resonant frequency of ~8-9 KHz and a signal amplitude of <0.2 V. Typical scan frequencies were between 1 and 3 Hz and the images were sampled at the resolution of 256 × 256 points.

For the AFM study, the samples were prepared by transferring the monolayers of cholesterol and ceramide onto freshly cleaved HOPG. To achieve transfer, the HOPG substrate was horizontally lowered in contact with the monolayer. Immediately after the transfer, a drop of water was placed on the substrate to preserve the humidity of the monolayer during the handling of the sample.

Antibody purification

Immunolabeling experiments were carried out with the monoclonal IgM antibody 36A1. This antibody was raised and selected against crystals of cholesterol monohydrate (Perl-Treves et al., 1996). For blocking nonspecific sites of interaction a nonspecific antibody (48E1), of the same IgM isotype as 36A1, was used (Geva et al., 2003).

The antibody was purified from ascites fluid by affinity chromatography using an ImmunoPure IgM purification kit, according to the manufacturer's instructions. Only fractions with optical density >0.2 were pooled. The purified antibody was extensively dialyzed against PBS and stored at 4°C.

Fluorescent labeling of the antibody

The purified antibody (270 μl) was diluted in 1 N Na_2CO_3 buffer (30 μL, pH 9). Rhodamine_B isothiocyanate was dissolved in dry dimethylsulfoxide (40 μl, 1.0 mg/ml) and slowly added to the antibody solution under constant agitation over 1 h at room temperature. The solution was stored for 5 h at 4°C, then 1 M NH_4Cl (18 μL) was added followed by 90 min additional storage at 4°C.

The labeled antibody was separated from the free rhodamine by dialysis and subsequent filtration on a Centricon centrifugal filter device with a molecular weight cutoff of 100,000. After filtration, the labeled antibody was stored in the dark at 4°C.

The final concentration of the antibody was determined by amino acid analysis.

Immunolabeling of monolayers

Solutions of the individual lipids and their mixtures in chloroform were prepared at a total concentration of 10^{-4} M. The monolayers were prepared by depositing on the air/water interface an amount of the respective solution (not fluorescently labeled) that corresponds to a surface coverage of 90%, as estimated from the average molecular areas determined from their π-A isotherms. After the monolayer was allowed to equilibrate for 15 min, the water subphase (18.2 mΩ Millipore water) was exchanged for a PBS solution (2.5 mL) containing both labeled antibody (36A1, 0.5 μg/mL) and the nonspecific competitor (48E1, 5 μg/mL). The system was allowed to equilibrate for 30 min, and monitored directly under the epifluorescence microscope. The monolayers were then lifted from the air/water interface onto OTS-coated glass coverslips. To achieve transfer, the solid substrate was horizontally lowered in contact with the monolayer. OTS-coating of the glass cover slides was necessary for reproducible transfer of good quality monolayers, with correct orientation of the functional hydroxyl groups toward the solution. To lower background fluorescence, the coverslips were then washed three times by setting them onto a clean water surface. Care was taken that the monolayer did not dry at any stage of transfer, washing, or observation. Transferred monolayers were analyzed by epifluorescence microscopy.

To avoid changes in antibody concentration that could result from antibody aggregation, sets of the monolayers of cholesterol, ceramide, and their mixtures were observed during the same day. In the case that no epifluorescence signal was observed (the 60:40 cholesterol/ceramide mixture) using the same value of the exposure time, this value was increased by several steps to verify the existence of the monolayer.

Immunofluorescence experiments on supported monolayers were carried out following the same general procedure described above, with the difference that the lipid monolayers were first lifted onto the glass substrate and then incubated with the antibody solution. For the incubation step, the monolayer transferred to glass was laid for 30 min on the solution containing the antibody and subsequently rinsed as above.

RESULTS

Lipid components of the system

Mixed monolayers of cholesterol and ceramide were chosen as a model system for cholesterol-lipid interactions in lipid rafts for various reasons: the most important consideration is to get information on the packing of the monolayer backbone

chains, disregarding in a first stage any bulky headgroups. These emerge from the monolayer into the solution, most likely in a disordered partial layer. Besides, all the techniques available, including GIXD, immunolabeling and AFM, provide the best information on packed monolayers, and they would be impaired by bulky headgroups protruding from the monolayers.

For a first characterization of the molecular packing of the monolayers at the air/water interface, surface pressure-molecular area (π-A) isotherms of cholesterol, ceramide, and their mixtures were recorded; the isotherms of mixtures with cholesterol/ceramide molar ratios of 30:70 and 60:40 are reported, together with the isotherm for the pure components (Fig. 1).

The π-A isotherm of pure C16 ceramide shows a typical lipid-like behavior. The monolayer shows a smooth transition from an expanded state to a more condensed state upon compression.

The average molecular areas measured for cholesterol and ceramide are similar, but the cholesterol monolayer is much less compressible in the low-surface pressure range. Due to its steroid backbone, cholesterol is more rigid and even at high molecular areas the molecule is not tilted relative to the interface (Rapaport et al., 2001). The decrease in surface area down to 40 Å^2 with compression causes fusion of the cholesterol domains without any change in the tilt of the molecule.

The π-A isotherms of the mixed cholesterol/ceramide monolayers are intermediate between the two pure monolayers of cholesterol and ceramide.

GIXD data

A detailed description of GIXD applied to films on liquid surfaces has been given elsewhere (Als-Nielsen and Kjaer, 1989; Kuzmenko et al., 2001; Jensen and Kjaer, 2001; see also Materials and Methods). Briefly, the monolayers are illuminated with an incident x-ray beam at a grazing angle from the surface lower than the critical angle for total reflection. The refracted (evanescent) beam, traveling parallel to the interface, is diffracted by the ordered organic film resulting in diffraction peaks (Bragg peaks). The diffraction pattern from the monolayer can be interpreted as resulting from a two-dimensional ''powder'' of crystallites all parallel to the water surface but randomly oriented around the surface normal. As the film has a monomolecular thickness, the intensity distribution in the z direction, perpendicular to the surface, appears as a continuum in the form of Bragg rods. Measurements were performed by scanning the horizontal component q_{xy} and resolving the out-of-plane component q_z, of the scattering vector $\boldsymbol{q}$ (see Methods).

The GIXD pattern is represented in two different ways. The intensity profile of each Bragg peak, $I(q_{xy})$, is obtained by integrating over q_z, whereas the Bragg rod intensity profiles $I(q_z)$ are integrated across the q_{xy} range of each diffraction peak separately for each q value. The q_{xy} positions of the Bragg peaks yield the lattice repeat distances $d = 2\pi/q_{xy}$, which may be indexed by the two Miller indices h,k to yield the unit cell. The full width at half maximum (FWHM) of the diffraction peaks yields the lateral two-dimensional crystalline coherence length $L_{xy} = 0.9(2\pi)/\mathrm{FWHM}(q_{xy})$. The width of the Bragg rod profile along q_z similarly gives a first estimate of the thickness of the crystalline film $L_z = 0.9(2\pi)/\mathrm{FWHM}(q_z)$.

All the GIXD data were recorded just at the point before the surface pressure began to rise. The corresponding molecular areas were in the range 38.5-40 Å^2, except for pure ceramide that was between 40 and 45 Å^2.

Structure of monolayers of ceramide

The GIXD pattern of pure ceramide in the uncompressed state (Fig. 2, *a* and *b*), with an area/molecule of 45 Å^2, displays three overlapping diffraction peaks (at $q_{xy} = 1.45_1$, 1.49_4, and 1.53_8 Å^{-1}) and an additional weak peak at $q_{xy} = 1.62$ Å^{-1}. An identical GIXD pattern—but for the weak peak, which was absent—was obtained for a 40:60 cholesterol/ceramide mixture with a molecular area of 45 Å^2. This film was then compressed to a molecular area of ~40 Å^2, with no observable surface pressure. The GIXD measurements, performed ~2 h later (Fig. 2, *c* and *d*), showed a phase change, albeit minor, coupled with a dramatic sharpening of the diffraction peaks (cf. Fig. 2, *a* and *c*), indicative of increased crystal domain size. Interestingly, these well-resolved diffraction peaks ($q_{xy} = 1.43_4$, 1.48_6, and 1.62_5 Å^{-1}, corresponding to a unit cell $a_2 = 5.18$ Å, $b_2 = 7.74$ Å, $\gamma_2 = 92.2°$), are very similar to those ($q_{xy} = 1.43_2$, 1.48_0, and 1.60_3 Å^{-1}) recently reported for a monolayer film of D-erythro-C18-ceramide at 18°C (Vaknin and Kelley, 2000). We thus focused upon the GIXD pattern of the 40:60 cholesterol/ceramide mixture (Fig. 2, *c* and *d*) for structure determination. We may now interpret the spectrum of pure ceramide as being composed of a main phase 1 (with cell dimensions $a_1 = 5.02$ Å, $b_1 = 8.17$ Å, $\gamma_1 = 91.9°$) and a minor phase 2 identical to that of the 40:60 mixture. The FWHM of the Bragg rods along q_z in the two phases (Fig. 2, *b* and *d*) are indicative of a monolayer thickness of ~20 Å.

The near-rectangular unit cell derived from Fig. 2, *c* and *d*, contains one independent molecule of ceramide. A rectangular unit cell of dimensions 5×7.5 Å^2 is fingerprint evidence of a herring-bone arrangement of hydrocarbon chains related by glide symmetry, with their chain axes aligned normal to the surface plane (Kuzmenko et al., 1998). In the case described here, the positions of the maxima along q_z of the three Bragg rods indicates that the chains are titled from the surface normal by an angle of ~14° in the direction of the *a*-axis (Kjaer,1994; Jensen and Kjaer, 2001). The dimensions of the unit cell projected onto a plane perpendicular to the molecular axis are $a \cos t \times b = 5.02 \times 7.74$ Å^2, in complete agreement with the two chains of the molecule forming a herring-bone arrangement related by pseudoglide symmetry. (The ceramide molecule is chiral of unique

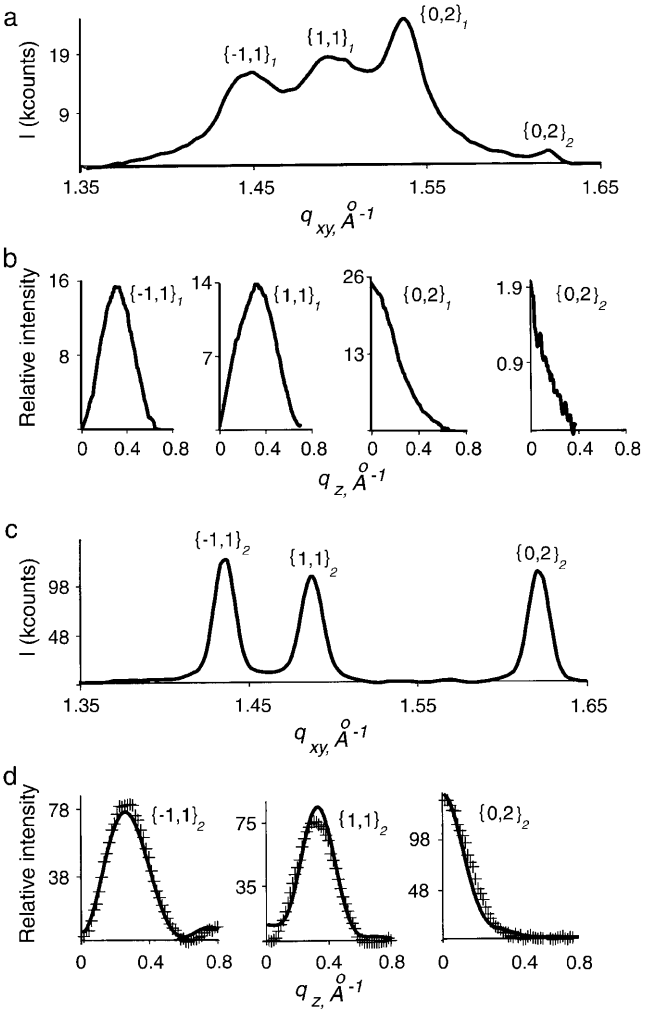

FIGURE 2 GIXD patterns of a monolayer of ceramide at the air/water interface under negligible surface pressure. (*a* and *b*) The diffraction peaks $I(q_{xy})$ and corresponding Bragg rods $I(q_z)$ of pure ceramide. The three peaks, indexed $\{h,k\}_1$, belong to phase 1. The weak peak, indexed $\{0,2\}_2$, belongs to phase 2. (*c* and *d*) The diffraction peaks $I(q_{xy})$ and corresponding observed (++) and calculated (—) Bragg rods $I(q_z)$ of ceramide from a 40:60 cholesterol/ceramide mixture, belonging to phase 2. The calculated curves were determined from the monolayer crystal structure (Fig. 3, *b* and *c*).

handedness. Its two chains cannot therefore be related by a crystallographic glide symmetry, which incorporates a mirror operation. Hence the description ''pseudoglide''.)

The molecular structure of cerebroside (Pascher and Sundell, 1977) was chosen as an initial model for determining the two-dimensional crystalline structure of ceramide. This molecular structure, constrained as a rigid body, was refined via SHELX by x-ray structure factor computations (see Method in Rapaport et al., 2001), yielding a reasonable fit between the observed and calculated Bragg rods (Fig. 2 *d*). The resulting packing arrangement (Fig. 3, *b* and *c*) incorporates molecules interlinked by N-H···O hydrogen bonds along the *a* axis. The thickness of the ceramide monolayer, according to Fig. 3 *c*, is 20.7 Å.

Structure of monolayers of cholesterol/ceramide mixtures

The GIXD patterns of mixtures of up to 30% ceramide with cholesterol, measured in the uncompressed state, are very similar to each other, containing peaks arising from ceramide only. In contrast, cholesterol and its mixtures with ceramide in molar ratios ranging from 90:10 to 67:33, measured both uncompressed and at pressures from 30 to 14 mN/m, show one diffraction peak (Fig. 4 *a*).

For pure cholesterol this diffraction peak of *d*-spacing 5.7 Å corresponds to the $\{1, 1\}$, $\{\bar{2}, 1\}$, and $\{1, \bar{2}\}$ reflections of a supercell of dimensions $a = b = 11.4$ Å (the symbol $\{h,k\}$ refers to both reflections (h,k) and $(-h,-k)$). In this supercell the cholesterol molecule is aligned normal to the water surface in a two-dimensional crystal of plane symmetry *p3* yielding an area/molecule of 38 $Å^2$ (Rapaport et al., 2001). In this structure (Fig. 3 *a*) the exocyclic chains are disordered. Introduction of increasing amounts of ceramide has multiple effects: the peak maximum is progressively shifted to higher values of q_{xy} (Figs. 4 *a* and 5 *a*), corresponding to a shrinkage of the area per molecule in the unit cell from 38 $Å^2$ to 30 $Å^2$ (Fig. 5 *b*). Since the cross-sectional area of ceramide is 40 $Å^2$, a reduction in the average area/molecule in the mixed crystal can only be achieved if one chain of ceramide (out of two) replaces one molecule of cholesterol, with a concomitant change in packing structure. The coherence length, reflecting the size of the crystalline domains, is drastically reduced from 75 Å for pure cholesterol to 35 Å for a 90:10 cholesterol/ceramide mixture, after which it remains unchanged (Fig. 5 *c*). In contrast, the integrated intensity of the diffraction peak is not affected by the introduction of 10% ceramide in the structure, but thereafter substantially decreases upon each further addition (Fig. 5 *d*). This is understandable because in the host-guest cholesterol/ceramide solid solution each molecular site is composed, on average, of both cholesterol and ceramide, so that substitutional and displacive disorder decreases the diffracted intensity. The thickness of the monolayer is little affected by the presence of ceramide as additive (Fig. 5 *e*).

In the range of compositions of cholesterol/ceramide of 67:33 to 30:70, the GIXD pattern of the mixtures show the diffraction of ceramide together with a weak broad Bragg peak corresponding to the new phase. As an example, the diffraction pattern of a 40:60 mixture is shown in Fig. 4 *b*.

Atomic force microscopy of ceramide monolayers

Complementary information about the thickness and morphology of the ceramide monolayers was obtained by AFM. For the purpose of performing AFM measurements, the monolayers were transferred onto graphite slides. Graphite was preferred over mica because intact monolayers can be lifted on the hydrophobic graphite by lowering the slides parallel to the monolayer and touching the surface from the air side. The use of mica slides tends to induce rearrangement

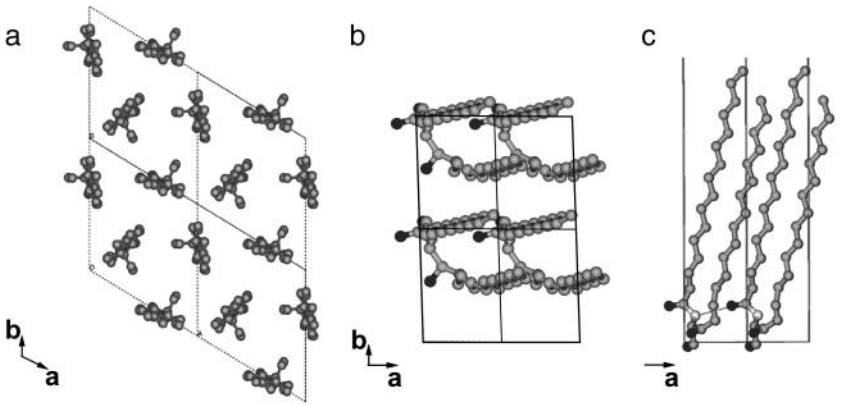

FIGURE 3 Molecular packing arrangement of (*a*) a monolayer of pure cholesterol (taken from Rapaport et al., 2001); (*b*) a monolayer of pure ceramide viewed along the normal to the layer plane; and (*c*) a monolayer of pure ceramide viewed along the *b* axis. Atoms: C, *shaded*; O, *black*; N, *white*. The hydrogen bond is marked by a dotted line.

of the monolayers, turning them upside-down to match the hydrophilic surface with their hydrophilic side. This generates patchy multilayer structures. In contrast, monolayers transferred onto graphite display large monolayer regions, alongside some multilayer regions. The latter can be easily detected by their increased height profiles.

Coexistence of two types of domains is observed within the transferred uncompressed monolayer of ceramide (Fig. 6, *left*). In uncompressed monolayers, 61% of the height profile measurements yielded a thickness of 14.7 ± 0.8 Å, 39% a thickness of 20.1 ± 0.8 Å. Upon compression to 20 mN/m, the morphology of the ceramide monolayer becomes more homogeneous, with a predominant type of domain of thickness 20.6 ± 0.9 Å being observed in 94% of the measurements, and of thickness 15.8 ± 0.2 Å in only 6% of the measurements (Fig. 6, *right*).

Immunofluorescence

Interaction of antibody 36A1 with monolayers of cholesterol and ceramide

Monoclonal antibody 36A1 was raised and selected against cholesterol monohydrate crystals, and it was found to interact at the air/water interface with cholesterol monolayers (Izhaky and Addadi, 1998, 2000).

After purification by affinity chromatography, the antibody was fluorescently labeled by covalent binding of a chromophore (rhodamine_B isothiocyanate). Nonfluorescent monolayers were incubated with the labeled antibody, in the presence of a nonlabeled competitor in 10-fold excess to avoid nonspecific adsorption. The competitor is a different IgM monoclonal antibody, which does not interact specifically with cholesterol-ordered arrays. Any fluorescence observed at the air/water interface under these conditions is due to the binding of the labeled antibody to the monolayer. The labeled monolayer/antibody complexes were then lifted onto glass slides and visualized under the epifluorescence microscope. Labeled monolayers observed while still at the air/water interface display the same features as monolayers observed after lifting onto glass slides (Izhaky and Addadi, 1998). It is, however, difficult to record images of monolayers at the air/water interface because of the high background fluorescence of the labeled antibody in solution. Furthermore, the uncompressed monolayer at the air/water interface is very mobile, thus making good pictures even more difficult to achieve. Representative images of uncompressed

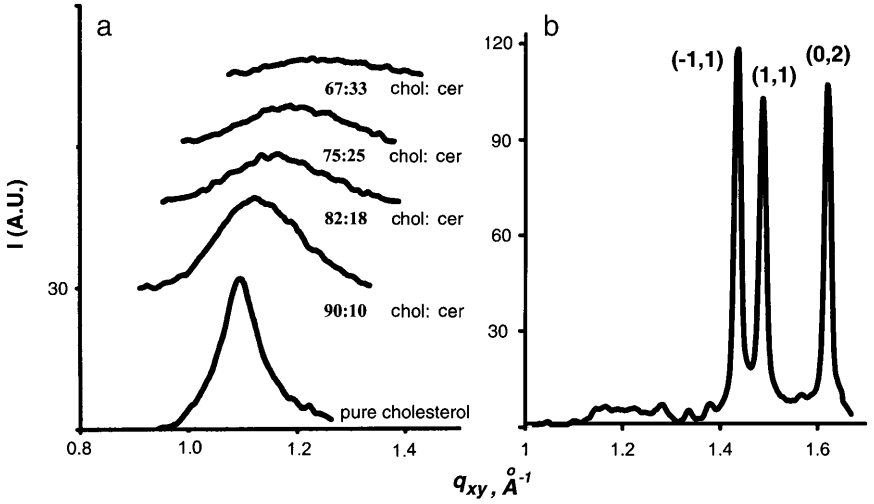

FIGURE 4 GIXD patterns of mixed cholesterol/ceramide monolayers. (*a*) Diffraction peak $I(q_{xy})$ as a function of ceramide content in the monolayer up to 33%. For convenience, the peaks are shifted along the vertical axis. (*b*) Diffraction pattern $I(q_{xy})$ of the 40:60 cholesterol/ceramide mixture displaying the three diffraction peaks of ceramide (*right*), which start to appear at compositions >33% ceramide, together with the diffraction peak of the cholesterol/ceramide phase (*left*, as in *a*). The intensity scale for the diffraction peaks in *a* is slightly larger than in *b*.

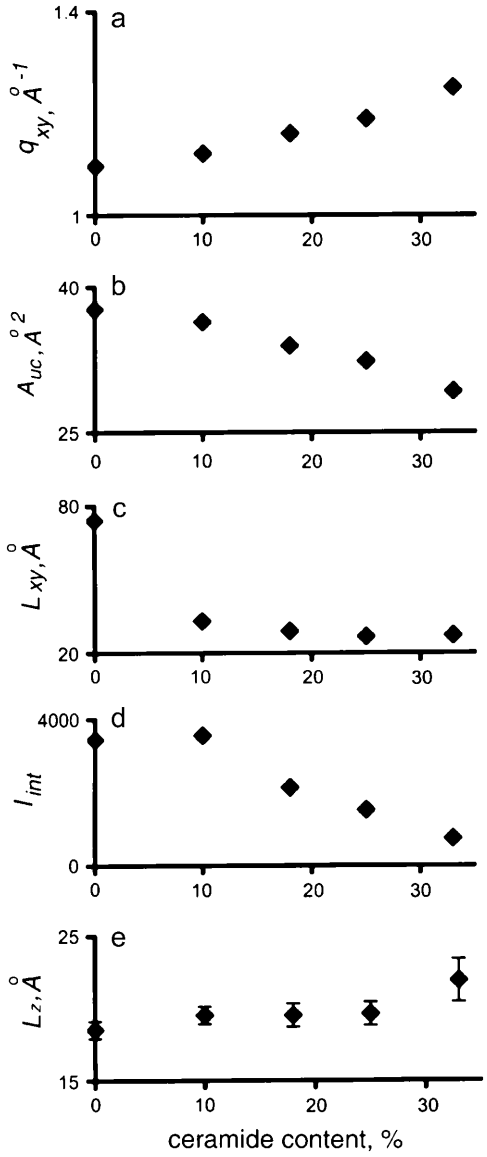

FIGURE 5 Dependence of crystalline parameters derived from the GIXD single diffraction peak on ceramide content in the mixed monolayers. (*a*) q_{xy}, position of the in-plane scattering vector. (*b*) A_{uc}, unit cell area. (*c*) L_{xy}, coherence length of the crystalline domains. (*d*) I_{int}, integrated intensity of the diffraction peak. (*e*) L_z, thickness of monolayer.

cholesterol and ceramide are presented in Fig. 7, *a* and *b*, at the same antibody concentration (0.5 μg/ml).

Antibody 36A1 binds to monolayers of cholesterol uniformly and specifically (Geva et al., 2001; Izhaky and Addadi, 2000). The antibody-bound cholesterol monolayers (Fig. 7 *a*) displayed their well-known morphological characteristics, i.e., a homogeneously fluorescent layer interrupted by small circular dark regions of empty interface.

The interaction of antibody 36A1 with the monolayer of C16 ceramide resulted in distinct patterns of dark and fluorescent patches (Fig. 7 *b*). The dark areas appear as rigid shapes with straight boundaries, suggesting the presence of a crystalline phase. Their appearance as dark regions suggests that the antibody does not interact with the ordered structure formed by molecules packed in a lattice (Geva et al., 2001; Okonogi and McConnell, 2004).

The fluid phase of the monolayer, in contrast, is more flexible, enabling nonspecific interactions with the antibody and resulting in fluorescent domains. This suggests partitioning of the antibody under the monolayer phases, driven by structural parameters.

To verify this hypothesis, immunofluorescence labeling of compressed and uncompressed ceramide monolayers was performed after lifting onto glass slides (Fig. 7, *c* and *d*). Incubation of the uncompressed monolayer with antibody after transferring onto the slide results in micrographs showing the same features as uncompressed monolayers incubated at the air/water interface and then lifted onto glass (compare Fig. 7, *b* and *c*). This is further evidence that lifting does not modify the monolayer organization. Upon compression to 20 mN/m, labeling of the ceramide monolayers was almost completely suppressed. This confirms the coexistence of ordered and disordered phase in uncompressed ceramide, with the percentage of the crystalline component increasing at higher compression.

These results are in agreement with the morphological mapping of the monolayers by atomic force microscopy. The two phases with heights of ~20 Å and ~15 Å observed by AFM can be attributed to the crystalline and disordered domains, respectively, which interact to a different extent with the labeled antibody, whereas the morphology of the compressed film of ceramide shows a unique thickness, corresponding to the ordered phase, which does not interact with the antibody.

Interaction of antibody 36A1 with mixed monolayers of cholesterol and ceramide

Next, the interaction of antibody 36A1 with mixed monolayers of cholesterol and ceramide was tested. Two mixtures, 60:40 cholesterol/ceramide and 30:70 cholesterol/ceramide, were studied.

The ceramide-rich mixture (Fig. 7 *f*) shows a fluorescent pattern similar to that of the ceramide monolayer, i.e., partitioning in dark and fluorescent domains due to different binding of the antibody to parts of the monolayer.

However, at the same antibody concentration, no fluorescent labeling of the 60:40 cholesterol/ceramide was observed (Fig. 7 *e*). This lack of fluorescence suggests the absence of any interaction between the antibody and this mixture, implying the formation of a homogeneous mixed phase with new properties that the antibody does not recognize.

DISCUSSION

The structures of cholesterol/ceramide mixtures in monolayers deposited at the air/water interface were determined.

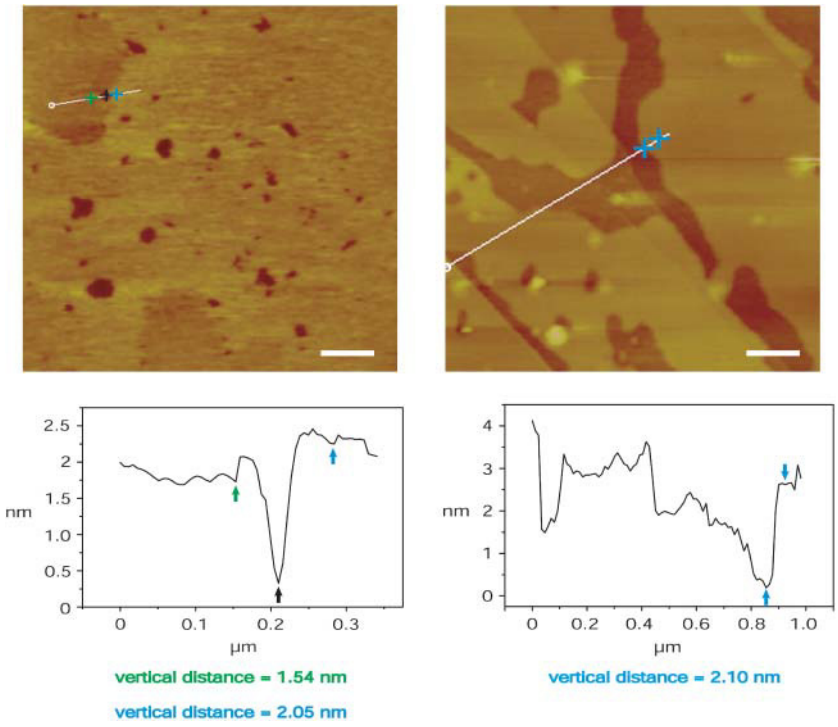

FIGURE 6 (*Top*) AFM height images of (*left*) uncompressed and (*right*) compressed ceramide monolayers imaged in water. The scale bar is 0.4 μm in both images. (*Bottom*) Height profiles along the continuous lines marked in the top panels.

In particular, we show here that mixtures in the composition range of 90:10–67:33 form a homogeneous new phase. This is characterized by crystalline domains of structure resembling that of pure cholesterol monolayers, with ceramide introduced as a solid solution and progressively modifying the structure. The model, derived from combined GIXD, AFM, and immunolabeling data, constitutes a first step toward the goal of building structural models that may be relevant in the future to the understanding of the organization of lipid rafts.

At zero pressures, pure ceramide monolayers crystallize primarily in a near-rectangular unit cell ($a = 5.02$ Å, $b = 8.17$ Å, $\gamma = 91.9°$). A 40:60 cholesterol/ceramide mixture was found to also crystallize in this same structure, but with time underwent a minor change to a much more crystalline structure. This crystalline phase (Fig. 2, *c* and *d*) forms a near-rectangular unit cell ($a = 5.18$ Å, $b = 7.74$ Å, $\gamma = 92.2°$), where two chains of the ceramide molecule, forming a herring-bone arrangement, are related by pseudoglide symmetry. Three diffraction peaks with q_{xy} values very similar to those obtained in Fig. 2 *c* were observed in a recent GIXD study of D-erythro-C18-ceramide (Vaknin and Kelley, 2000) carried out on a monolayer film of the pure material at 18°C. In this study the corresponding Bragg rods, along q_z, were not reported. The three peaks were attributed to two coexistent crystalline phases, one hexagonal and the other orthorhombic ($a = 5.30$ Å, $b = 7.84$ Å). Although the data of Vaknin and Kelley may be interpreted as reported, given the experimental data available, we deem our model for the zero-pressure phase reliable, because all three observed Bragg rods were well fitted by a single crystalline phase. It is conceivable, based on the fact that the structure was observed here in a 40:60 cholesterol/ceramide mixture, that the presence of cholesterol further stabilizes this structure in the given composition range.

Although GIXD is the most reliable method of determining the size and structure of the crystalline arrays, it does not alone provide information about possible coexisting amorphous phases in the monolayer. Fluorescence immunolabeling and AFM were thus used as complementary techniques to more fully characterize the phases present in the monolayer.

In ceramide monolayers, immunofluorescence confirmed the existence of a crystalline phase that is not labeled by the antibody, intermixed with an additional amorphous phase that was nonspecifically labeled by the antibody. The latter phase disappeared upon compression of the monolayer, thus supporting the notion that it is disordered and more relaxed than the crystalline phase.

Antibody 36A1 was selected by interaction with cholesterol monohydrate crystals (Perl-Treves et al., 1996). Its variable domain was sequenced and the structure of its active site was modeled. The binding site model assumes the shape of a step, with one hydrophilic side lined by five hydroxyl groups, whereas the other side is paved by hydrophobic residues. These match well the hydroxyl headgroups and hydrophobic backbone, respectively, of cholesterol molecules exposed at the corresponding step on the cholesterol crystals. The antibody was observed to bind to cholesterol monolayers, which display at the water interface a packing arrangement similar to that specifically recognized on the crystal steps. We suggest that the antibody does not interact

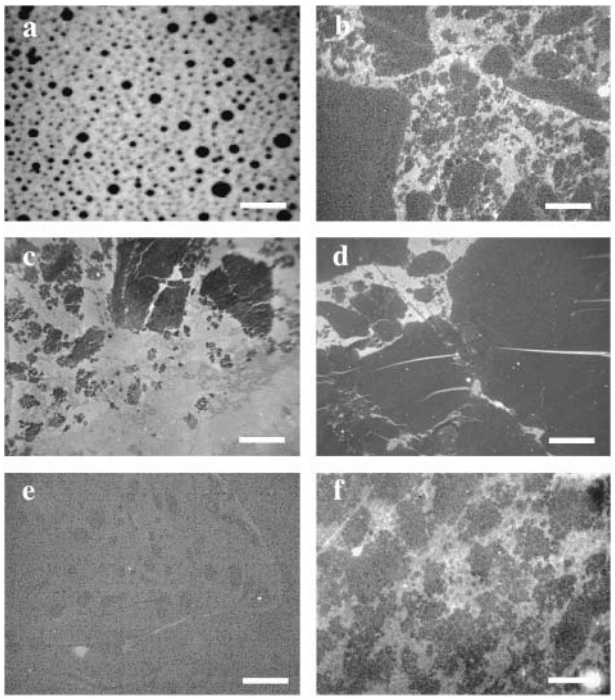

FIGURE 7 Epifluorescence micrographs of antibody-bound monolayers of (*a*) uncompressed cholesterol; (*b*) uncompressed ceramide; (*c*) uncompressed ceramide; (*d*) compressed ceramide; (*e*) 60:40 cholesterol/ceramide; and (*f*) 30:70 cholesterol/ceramide . The monolayers in *a*, *b*, *e*, and *f* were incubated with the antibody in the trough and the monolayers in *c* and *d* were incubated with the antibody after lifting onto a glass slide. The concentration of the antibody in *a*, *b*, *e*, and *f* is 0.5 μg/mL and in *c* and *d* is 1 μg/mL. Scale bar, 40 μm.

with the crystalline part of the monolayers of ceramide, because their packing is different from that of the specifically recognized cholesterol motif. The interaction with the amorphous phase is attributed to interaction with the hydroxyl and aliphatic groups of ceramide, made possible by the ''loosely packed disordered'' phase. The same labeling pattern of exclusion from crystalline domains and labeling of disordered domains was observed with triacontanol, a long-chain aliphatic alcohol also forming monolayers comprising a crystalline and a disordered phase (Geva et al., 2001).

We note that the loosely packed character of the amorphous phase is further confirmed in the GIXD analysis of our data and that of Vaknin and Kelley. At the area/molecule derived for the crystalline phase from the diffraction data ($\approx$40 Å^2), the monolayer surface pressure would be 18 mN/m (Fig. 1). The surface pressure being zero, a higher average molecular area must be assumed, indicating the presence of an additional expanded phase.

AFM studies confirmed that both the crystalline phase and the disordered phase are single molecular layers. The uncompressed monolayer is formed of two types of domains, characterized by a thickness of $\sim$20 and $\sim$15 Å. The 20-Å thickness matches the length of a C16 ceramide molecule (sphingosine base linked through an amide to a palmitic acid) oriented vertical to the surface, indicating that this is the crystalline phase monitored by GIXD and not labeled by the antibody. The 15-Å high domains indicate that the molecules are highly tilted relative to the normal of the surface, in a poorly packed arrangement that corresponds to the disordered phase labeled by the antibody. After compressing the monolayer, the more ordered domains become prevalent, confirming once more that the 20-Å thick phase of the ceramide monolayer is the crystalline one.

Although we are well aware of the differences that may be induced in the monolayer organization by lifting onto a solid support, we are convinced, to the best of our knowledge, that these differences do not influence our conclusions, insofar as artifacts due to lifting are easily detectable both in AFM and by immunofluorescence. Furthermore, monolayers incubated with antibody before and after lifting have the same features, indicating that the epitope of antibody binding did not change, either in molecular organization or in availability to binding.

Addition of small amounts of cholesterol to ceramide did not induce changes in the GIXD pattern of these mixtures up to a 30:70 ratio of cholesterol/ceramide. Since the crystalline phase of pure ceramide is highly ordered, and cholesterol is a rigid molecule that cannot easily adapt to the packing of ceramide, we tend to believe that cholesterol does not enter the ceramide structure. Cholesterol should thus be rather present in a dispersed form that does not contribute to the diffraction pattern. In contrast, mixed monolayers of cholesterol/ceramide in the composition range of 90:10–67:33 form a new unique phase, represented in GIXD by a broad diffraction peak. By the same logic as above, ceramide, being flexible, can accommodate within the less well-ordered phase of cholesterol. Upon progressive addition of ceramide to cholesterol, the maximum of the peak corresponding to pure cholesterol shifts to higher values of q_{xy}, the peak broadens, and its intensity decreases, corresponding to a decrease in the size of the crystalline domains and in their crystallinity. Such a decrease in intensity and structure can be due either to a destructive x-ray interference from the two components or to formation of an amorphous phase.

We checked for the possible existence of such putative amorphous regions by immunofluorescence experiments carried out on mixed monolayers. The fluorescent images show different patterns, depending on the ratio between the two lipid components. At a cholesterol/ceramide ratio of 30:70, the labeled monolayer shows distinct dark and fluorescent regions, illustrating a lipid demixing (Fig. 7 *f*). Since ceramide is in excess, we attribute the fluorescence to ceramide-rich disordered domains that form a separate phase. In contrast with this, and in agreement with the GIXD data, no fluorescent labeling of the 60:40 mixture of cholesterol/ceramide was observed (Fig. 7 *e*). This sort of ''negative labeling'' indicates the lack of interaction between the antibody and the monolayer, together with the absence of any amorphous phase of ceramide that would have been fluorescent. The lack of interaction between the antibody and the

new phase stresses the antibody sensitivity to chemical and structural parameters even only slightly different from the cholesterol monolayer, which the antibody does recognize. Thus, the immunofluorescence experiments on monolayers supports the idea of a new and homogeneous phase.

The single GIXD peak that characterizes the new phase is a clear signature of threefold symmetry; therefore, the ceramide molecules that enter the cholesterol unit cell preserve the *p*3 lattice of cholesterol, containing three molecules related by threefold symmetry. An approximate molecular area of 30 $Å^2$, measured for the 67:33 cholesterol/ceramide mixture can be obtained only if one chain of ceramide, with a cross-sectional area of 20 $Å^2$, which is half the cross-sectional area of ceramide, will replace one molecule of cholesterol with a cross-sectional area of 38 $Å^2$. The average distance between neighboring cholesterol sites is 5.9 Å, whereas the distance between two ceramide chains in ceramide's monolayer crystal structure (Fig. 3, *b* and *c*) is ≈5 Å; that is, the two chains can almost span the distance between two cholesterol molecular sites. The unit cell of the mixture will thus contain on average 1.5 mol of cholesterol and 0.75 molecules of ceramide over the three molecular sites in a unit cell, shrunk relative to that of cholesterol. The measured coherence length for a 67:33 mixture is 30 Å, corresponding to an area of 700 $Å^2$, and thus to domains containing ~25 molecules (Fig. 8).

We note that in the solid state, ceramide and cholesterol form eutectic mixtures in the range where a unique homogeneous phase was observed in monolayers (Ohta and Hatta, 2002). Obviously, the three-dimensionality of the bulk phase introduces additional constraints to the packing of molecules, relative to single molecular layers.

Ceramide was selected for structural studies here, despite it being a less abundant component of lipid rafts relative to other sphingolipids with larger headgroups, such as sphingomyelin. The ceramide backbone is, however, shared by all sphingolipids. As this is the part of the molecules that interacts directly with the cholesterol backbone in the membrane bilayers, it was selected here as a candidate to study the basic packing modes of the mixtures.

Clearly, the system is drastically simplified. In addition, monolayers were addressed, rather than the bilayers of membranes. No claim can thus possibly be made concerning a direct relevance of the observed structure to lipid rafts. It is interesting, however, to note data in the recent literature indicating some potential relevance of the present model of cholesterol/ceramide mixtures to the arrangement of lipid rafts. Wang and Silvius (2003) measured dramatically higher affinity of ceramide for ordered lipid domains in cholesterol-containing bilayers. Their data also suggest that sphingolipids with a variety of headgroup structures will be enriched in liquid-ordered regions of membranes, in a manner that is only modestly dependent on the nature of the polar headgroup. Ceramide is predicted to show a particularly strong enrichment in such domains. Radhakrishnan, Anderson and McConnell (2000) detect the presence in cholesterol-phospholipid monolayers of ''condensed complexes'' of cholesterol and sphingolipids. Interestingly, each complex contains 15–30 molecules, in excellent agreement with the phase observed here. In addition, independent information collected on lipid rafts converge to a consensus cholesterol/sphingolipid ratio of ~2:1 (Edidin, 2003; Pike, 2003).

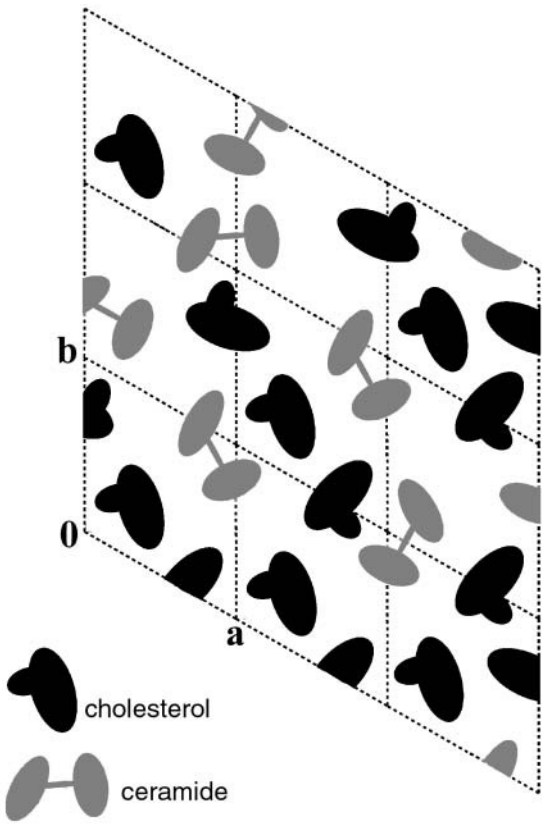

FIGURE 8 Schematic model of monolayer molecular arrangement of the 67:33 cholesterol/ceramide mixture. Two chains of an occluded ceramide molecule replace two molecules of cholesterol separated by ~6 Å in the monolayer structure of pure cholesterol (Fig. 3 *a*), so reducing the average ''molecular'' area from 38 $Å^2$ to 30 $Å^2$ in the mixture. The scheme contains ~25 molecules, representing the average domain size of the mixed new phase.

We have shown that antibodies raised and selected to recognize crystalline arrangements of cholesterol can be used to label similar crystalline or paracrystalline domains of cholesterol in the membrane of cholesterol-enriched cells (Kruth et al., 2001).

To directly test the relevance of the crystalline arrangement observed in the mixed monolayers to lipid rafts, we are planning in the next step to produce, select, and characterize monoclonal antibodies that specifically recognize the structural features of the mixtures. These will then be applied to cell membranes as reporters of the presence of the same arrangements in lipid rafts.

We thank Merav Geva for helpful advice and fruitful discussions. We thank HASYLAB for synchrotron beamtime. L.A. is incumbent of the Dorothy

and Patrick Gorman professorial chair, and L.S. is the recipient of the Eshkol Fellowship, administered by the Israel Ministry of Science.

This work was supported by a grant from the Israel Science Foundation, administered by the Israel Academy of Sciences, the Kimmelmann Center, and the DanSync program of the Danish Natural Science Research Council and the European Community under TMR-Contract ERBFMGECT950059.

REFERENCES

Addadi, L., M. Geva, and H. S. Kruth. 2003. Structural information about organized cholesterol domains from specific antibody recognition. *Biochim. Biophys. Acta*. 1610:208–216.

Als-Nielsen, J., and K. Kjaer. 1989. X-ray reflectivity and diffraction studies of liquid surfaces and surfactant monolayers. *In* Phase Transitions in Soft Condensed Matter. T. Riste and D. Sherrington, editors. Plenum Press, New York. 113–138.

Brown, D. A., and E. London. 1997. Structure of detergent-resistant membrane domains: does phase separation occur in biological membranes? *Biochem. Biophys. Res. Commun.* 240:1–7.

Brown, D. A., and J. K. Rose. 1992. Sorting of GPI-anchored proteins to glycolipid-enriched membrane subdomains during transport to the apical cell surface. *Cell*. 68:533–544.

Edidin, M. 2003. The state of lipid rafts: from model membranes to cells. *Annu. Rev. Biophys. Biomol. Struct.* 32:257–283.

Friedrichson, T., and T. V. Kurzchalia. 1998. Microdomains of GPI-anchored proteins in living cells revealed by crosslinking. *Nature*. 394: 802–805.

Geva, M., F. Frolow, M. Eisenstein, and L. Addadi. 2003. Antibody recognition of chiral surfaces. Enantiomorphous crystals of leucine-leucine-tyrosine. *J. Am. Chem. Soc.* 125:696–704.

Geva, M., D. Izhaky, D. E. Mickus, S. D. Rychnovsky, and L. Addadi. 2001. Stereoselective recognition of monolayers of cholesterol, ent-cholesterol, and epicholesterol by an antibody. *ChemBioChem.* 2:265–271.

Giocondi, M. C., V. Vie, E. Lesniewska, J. P. Goudonnet, and C. Le Grimellec. 2000. In situ imaging of detergent-resistant membranes by atomic force microscopy. *J. Struct. Biol.* 131:38–43.

Huang, J., and G. W. Feigenson. 1999. A microscopic interaction model of maximum solubility of cholesterol in lipid bilayers. *Biophys. J.* 76:2142–2157.

Izhaky, D., and L. Addadi. 1998. Pattern recognition by antibodies for two-dimensional arrays of molecules. *Adv. Mater.* 10:1009–1014.

Izhaky, D., and L. Addadi. 2000. Stereoselective interactions of a specialized antibody with cholesterol and epicholesterol monolayers. *Chemistry*. 6:869–874.

Jensen, T. R., and K. Kjaer. 2001. Structural properties and interactions of thin films at the air-liquid interface explored by synchrotron X-ray scattering. *In* Studies in Interface Science, Vol. 11. Novel Methods to Study Interfacial Layers. D. Moebius and R. Miller, editors. Elsevier, Amsterdam. 205–254.

Kessler, N., D. Perl-Treves, and L. Addadi. 1996. Monoclonal antibodies that specifically recognize crystals of dinitrobenzene. *FASEB J*. 10:1435–1442.

Kessler, N., D. Perl-Treves, L. Addadi, and M. Eisenstein. 1999. Structural and chemical complementarity between antibodies and the crystal surfaces they recognize. *Proteins.* 34:383–394.

Kjaer, K. 1994. Some simple ideas on x-ray reflection and grazing-incidence diffraction from thin surfactant films. *Physica B*. 198:100–109.

Kruth, H. S., I. Ifrim, J. Chang, L. Addadi, D. Perl-Treves, and W. Y. Zhang. 2001. Monoclonal antibody detection of plasma membrane cholesterol microdomains responsive to cholesterol trafficking. *J. Lipid Res.* 42:1492–1500.

Kuzmenko, I., V. M. Kaganer, and L. Leiserowitz. 1998. Packing of hydrocarbon chains and symmetry of condensed phases in Langmuir monolayers. *Langmuir*. 14:3882–3888.

Kuzmenko, I., H. Rapaport, K. Kjaer, J. Als-Nielsen, I. Weissbuch, M. Lahav, and L. Leiserowitz. 2001. Design and characterization of crystalline thin film architectures at the air-liquid interface: simplicity to complexity. *Chem. Rev.* 101:1659–1696.

Majewski, J., T. L. Kuhl, K. Kjaer, and G. S. Smith. 2001. Packing of ganglioside-phospholipid monolayers: an x-ray diffraction and reflectivity study. *Biophys. J.* 81:2707–2715.

Ohta, N., and I. Hatta. 2002. Interaction among molecules in mixtures of ceramide/stearic acid, ceramide/cholesterol and ceramide/stearic acid/cholesterol. *Chem. Phys. Lipids*. 115:93–105.

Okonogi, T. M., and H. M. McConnell. 2004. Contrast inversion in the epifluorescence of cholesterol-phospholipid monolayers. *Biophys. J.* 86: 880–890.

Pascher, I., and S. Sundell. 1977. Molecular arrangements in sphingolipids: the crystal structure of cerebroside. *Chem. Phys. Lipids*. 20:175–191.

Perl-Treves, D., N. Kessler, D. Izhaky, and L. Addadi. 1996. Monoclonal antibody recognition of cholesterol monohydrate crystal faces. *Chem. Biol.* 3:567–577.

Pike, L. J. 2003. Lipid rafts: bringing order to chaos. *J. Lipid Res.* 44:655–667.

Pralle, A., P. Keller, E. L. Florin, K. Simons, and J. K. Horber. 2000. Sphingolipid-cholesterol rafts diffuse as small entities in the plasma membrane of mammalian cells. *J. Cell Biol.* 148:997–1008.

Radhakrishnan, A., T. G. Anderson, and H. M. McConnell. 2000. Condensed complexes, rafts, and the chemical activity of cholesterol in membranes. *Proc. Natl. Acad. Sci. USA*. 97:12422–12427.

Ramstedt, B., and J. P. Slotte. 2002. Membrane properties of sphingomyelins. *FEBS Lett.* 531:33–37.

Rapaport, H., I. Kuzmenko, S. Lafont, K. Kjaer, P. B. Howes, J. Als-Nielsen, M. Lahav, and L. Leiserowitz. 2001. Cholesterol monohydrate nucleation in ultrathin films on water. *Biophys. J.* 81:2729–2736.

Schneider, P. B., and E. P. Kennedy. 1967. Sphingomyelinase in normal human spleens and in spleens from subjects with Niemann-Pick disease. *J. Lipid Res.* 8:202–209.

Simons, K., and I. Ikonen. 1997. Functional rafts in cell membranes. *Nature*. 387:569–572.

Simons, K., and D. Toomre. 2000. Lipid rafts and signal transduction. *Nat. Rev. Mol. Cell Biol.* 1:31–39.

Singer, S. J., and G. L. Nicolson. 1972. The fluid mosaic model of the structure of cell membranes. *Science*. 175:720–731.

Smart, E. J., G. A. Graf, M. A. McNiven, W. C. Sessa, J. A. Engelman, P. E. Scherer, T. Okamoto, and M. P. Lisanti. 1999. Caveolins, liquid-ordered domains, and signal transduction. *Mol. Cell. Biol.* 19:7289–7304.

Vaknin, D., and M. S. Kelley. 2000. The structure of D-erythro-C18 ceramide at the air-water interface. *Biophys. J.* 79:2616–2623.

Varma, R., and S. Mayor. 1998. GPI-anchored proteins are organized in submicron domains at the cell surface. *Nature*. 394:798–801.

Wang, T. Y., and J. R. Silvius. 2003. Sphingolipid partitioning into ordered domains in cholesterol-free and cholesterol-containing lipid bilayers. *Biophys. J.* 84:367–378.

Xu, X., R. Bittman, G. Duportail, D. Heissler, C. Vilcheze, and E. London. 2001. Effect of the structure of natural sterols and sphingolipids on the formation of ordered sphingolipid/sterol domains (rafts). Comparison of cholesterol to plant, fungal, and disease-associated sterols and comparison of sphingomyelin, cerebrosides, and ceramide. *J. Biol. Chem.* 276: 33540–33546.